Surface electromagnetic waves in two-dimensional photonic crystals: Effect of the position of the surface plane

F. Ramos-Mendieta
Centro de Investigación en Física de la Universidad de Sonora, Apartado Postal 5-088, Hermosillo, Sonora 83190, Mexico

P. Halevi
Instituto Nacional de Astrofísica Optica y Electrónica, Apartado Postal 51, Puebla, Puebla 72000, Mexico
(Received 24 August 1998; revised manuscript received 8 March 1999)

A semi-infinite photonic crystal can support electromagnetic wave propagation at its surface. By using the supercell method, we studied in detail the properties of these (nonradiative) modes in crystals of two-dimensional periodicity constituted by parallel rods of square cross section. The rods cut the plane of periodicity (001) at the sites of a square lattice, and the sides of the rods have the same orientation as the lattice. We have performed calculations for crystals of air cylinders in a dielectric background. The Bloch-type surface waves are assumed to propagate at the (100) surface in the [010] direction. For both transverse electric and transverse magnetic polarizations, we found that the dispersion curves of the surface modes and their field confinements at the surface are strongly dependent on the crystal termination, that is, on the position of the cut plane through the rods. We also found that the degree of localization of the fields at the surface depends on the position of the mode within the band gap. Plots of the field intensity show that the TM waves are more strongly localized than the TE waves. [S0163-1829(99)08523-9]

I. INTRODUCTION

It is well known that the diffraction of electromagnetic waves in a photonic crystal gives rise to band structure for the eigenfrequencies. During the last decade, much theoretical and experimental work has proved that, depending on their design characteristics, photonic crystals can support frequency band gaps where electromagnetic oscillations are forbidden.[1,2] This property has potential applications in the optoelectronic industry and can lead to new fundamental phenomena.

It has been also shown that photonic crystals can support surface modes which propagate along the crystal-air interface. It has been suggested that by understanding the surface band structure the losses associated with radiation (due to localized sources) into surface modes could be eliminated.[3] The surface modes are characterized by decaying fields in both perpendicular directions away from the surface plane. On the air side the exponential decay of the field amplitude is a straightforward consequence of the propagation vector being greater than the vacuum wave vector. Inside the crystal the fields decay because interference effects. Thus the surface waves in photonic crystals are of different character than the well-known surface polaritons in a homogeneous half-space. In the latter case the decay in the material medium is caused simply by the negative value of its dielectric function.

Surface waves in photonic crystals are Bloch-type waves—the periodicity of the dielectric constant parallel to the surface plane requires application of the Bloch theorem. Such waves were found theoretically in a three-dimensional (3D) structure constituted of a set of dielectric columns connecting the sites of a diamond lattice.[3] The calculations showed that their dispersion curve $\omega=\omega(k_{\|})$ is strongly dependent on the position of the surface. It was also argued that surface electromagnetic modes always exist for some termination (position of the surface plane) in structures supporting complete band gaps. Experimentally, the surface waves were detected at gigahertz frequencies in a 2D array of parallel alumina ceramic rods of circular cross section.[4] In this crystal (square array exhibiting a full band gap $\Delta\omega\sim 25\,\mathrm{GHz}$), the surface waves were excited using the attenuated total reflection technique. In this experiment no evidence of surface modes was found for crystals terminated by complete rods. The surface modes were detected with the surface layer of cylinders cut in half (hemicylinders).

In this paper we investigate the properties of surface waves in 2D photonic crystals of square cylinders that form a square lattice. The crystals give rise to *complete* band gaps. In recent calculations[5] we have shown that surface modes may appear in incomplete, as well as in complete, gaps. In any case, surface modes are restricted to the right side of the vacuum light line and must lie within the band gaps of the surface bands—the projected bulk bands along the surface of interest. The light line satisfying $\omega=ck_{\|}$, where c is the speed of light in vacuum and $k_{\|}$ is the component of the wave vector parallel to the surface, separates the oscillatory ($\omega>ck_{\|}$) and the exponentially decaying ($\omega<ck_{\|}$) solutions for the fields in the perpendicular direction away from the surface on the air side. On the other hand, in the crystal the solutions with real $k_{\|}$ may have either real or complex perpendicular component $k_{\perp}$. The former—solutions with real $k_{\perp}$—give rise to the bulk modes. The latter—solutions with complex $k_{\perp}$—give rise to surface modes. This study is restricted to frequencies $\omega<\pi c/d$ (where d is the period in the direction of wave propagation), in which region the surface waves have nonradiative character. Above this frequency all solutions are necessarily radiative, which is to say that a surface wave is damped by radiating energy into air. A brief

discussion of radiative or leaky modes is given at the end of the paper.

In our calculations we use the plane-wave expansion for the electromagnetic fields. Surface modes are obtained by applying the Bloch theorem and by defining the appropriate supercell. A complete description of the method for 1D structures—dielectric superlattices—where the reliability of the supercell method was proved, has been published recently.[6] Rather than studying surface modes in a semi-infinite crystal, we calculate the surface modes in a crystal slab. The main idea of the method is the postulation of an auxiliary infinitely periodic superstructure constituted by crystal slabs alternating with air slabs. By using the Bloch theorem for this superstructure and taking into account the internal (photonic crystal) structure of the slabs, the wave equation is solved for $\omega(k_{\|})$, giving rise to a frequency band structure for oscillating solutions guided by the crystal slab. Some of these bands are constituted by modes which have maximum field amplitude near the crystal-air interfaces. Their fields decay exponentially into the air regions, and they become vanishingly small in the photonic crystal far enough from the surface. Thus these modes have surface-mode character. The width of the band is related to the coupling of all the neighboring surface modes in the auxiliary superstructure.

There are two requirements for an accurate computation of the surface modes. One is that the air regions be wide enough in order to ensure that the surface modes of any one crystal slab do not interact (overlap) with those of the neighboring slabs on each side. The other condition is that the crystal slab be sufficiently wide to guarantee the independence of the modes at its two surfaces. These requirements are satisfied provided that the widths of the air and the crystal regions are sufficiently greater than the decay lengths of the fields in the corresponding regions. If such limits are taken, then the dispersion curve obtained is expected to converge to the dispersion curve of the surface modes of the semi-infinite crystal. In this limit the surface mode solutions are infinitely degenerate.

It is known that the supercell method requires a very large number of waves in the expansion in order to represent adequately the dielectric function of the superstructure. We made calculations with a rectangular symmetric supercell containing seven or nine cells with the high dielectric contrast $\varepsilon_a/\varepsilon_0$ of 17.9. All the solutions that we shall present were obtained with a basis larger than 3200 plane waves, giving results with precision better than 95%.

The rest of the paper is organized as follows. In Sec. II we resolve the wave equation for both TE and TM waves with propagation vector in the plane of periodicity. General expressions to compute the bulk and surface bands are obtained. In Sec. III numerical results are presented. We investigate the properties of the surface modes as a function of the surface position and the polarization. In Sec. IV we give our conclusions.

II. CALCULATION OF THE BULK AND SURFACE MODES

We investigate wave propagation in 2D periodic dielectric structures, with the x,y plane being the plane of periodicity.

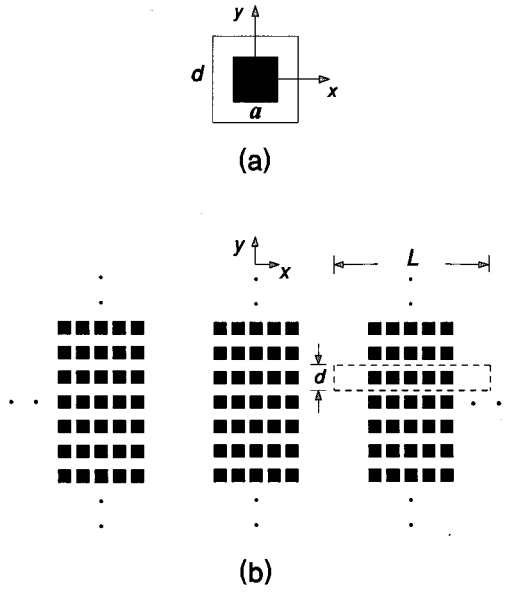

FIG. 1. (a) Square unit cell with sides of length d. The square cylinder at the center of the cell has dielectric constant ε_a. It is infinite in the z direction and is surrounded by another medium of dielectric constant ε_b. (b) Auxiliary superstructure for calculations of surface modes. It is constituted by crystal slabs alternated with air slabs. The supercell of area $A_c = Ld$ is shown by dashed lines.

The medium is homogeneous along the z axis, and the propagation vector is parallel to the plane of periodicity. We describe such structures by means of a periodic dielectric constant, namely, $\varepsilon(\mathbf{x}) = \varepsilon(\mathbf{x}+\mathbf{R})$, where both the position vector $\mathbf{x}$ and the lattice vector $\mathbf{R}$ lie in the plane x,y. We seek solutions for two structures. The first one is the infinite array—the 2D photonic crystal—of parallel rods of square cross section $s = a \times a$ with their axes cutting the x,y plane at the sites of a square lattice. The infinitely long rods are parallel to the z axis and are surrounded by air. The two-dimensional unit cell is square with sides of length d. A rod is placed at the cell center as shown in Fig. 1(a). The 2D periodic structure is generated by repeating the unit cell at the points $\mathbf{R}_{lm} = d(l\hat{i} + m\hat{j})$, with l and m integers.

The second structure, shown schematically in Fig. 1(b), has an auxiliary character and is used to obtain the surface modes of the photonic crystal. We have air slabs alternating with crystal slabs. It can be seen that the unit cell—the supercell—of length L along the x axis and width d along the y axis is more complicated. This centrosymmetric supercell contains n rods that are bounded by air regions. The $n-2$ inner rods have always the nominal square cross section s. Although in Fig. 1(b) the crystal slab in the supercell terminates with complete rods at the surfaces, it is possible to select a different surface position in order to leave incomplete exterior rods (see below). The infinite superstructure is generated by considering the supercell as the basis of the rectangular lattice $\mathbf{R}_{lm} = Ll\hat{i} + dm\hat{j}$, where l and m are integers.

With the propagation vector in the x,y plane, there are two independent vibration modes. These are the TE mode with the electric field parallel to the z axis and the TM mode with the electric field in the x,y plane. From Maxwell's equations we find the wave equations for the fields $E(x,y)$ (TE) and

$H(x,y)$ (TM), which are parallel to the cylinders:

$$\frac{1}{\varepsilon(x,y)}\nabla^2 E(x,y) = -\frac{\omega^2}{c^2}E(x,y), \tag{1}$$

$$\left[\frac{\partial}{\partial x}\frac{1}{\varepsilon(x,y)}\frac{\partial}{\partial x}+\frac{\partial}{\partial y}\frac{1}{\varepsilon(x,y)}\frac{\partial}{\partial y}\right]H(x,y) = -\frac{\omega^2}{c^2}H(x,y). \tag{2}$$

Because of the periodicity, the solutions of these equations are written so as to satisfy the Bloch theorem. By using a plane-wave basis, we expand both the inverse dielectric function and the cell-periodic part of the fields. After some algebraic manipulations one obtains

$$\sum_{\mathbf{G}'} \mu_{\mathbf{G}-\mathbf{G}'}|\mathbf{k}+\mathbf{G}'|^2 E_{\mathbf{G}'} = \frac{\omega^2}{c^2}E_{\mathbf{G}} \quad \text{(TE)}, \tag{3}$$

$$\sum_{\mathbf{G}'} \mu_{\mathbf{G}-\mathbf{G}'}(\mathbf{k}+\mathbf{G})\cdot(\mathbf{k}+\mathbf{G}')H_{\mathbf{G}'} = \frac{\omega^2}{c^2}H_{\mathbf{G}} \quad \text{(TM)}, \tag{4}$$

where $\mathbf{G}$ and $\mathbf{G}'$ are the reciprocal lattice vectors. The Fourier coefficient $\mu_{\mathbf{G}-\mathbf{G}'}$ is given by

$$\mu_{\mathbf{G}} = \frac{1}{A}\int_A \frac{d\mathbf{x}}{\varepsilon(\mathbf{x})}\exp(-i\mathbf{G}\cdot\mathbf{x}), \tag{5}$$

where A is the unit cell area.

The formulas (3) and (4) represent two infinite sets of equations for the eigenvectors $E_{\mathbf{G}}$ and $H_{\mathbf{G}}$. For given values of the Bloch wave vector $\mathbf{k}$, each set of equations has solutions for some eigenvalues $\omega_j(\mathbf{k})$ where the band index j $(=1,2,3,\ldots)$ specifies the serial number of a photonic band in ascending order of the frequency. These equations are valid for both dielectric structures described at the beginning of this section. In the first case (the infinite crystal), by running the wave vector $\mathbf{k}$ along the periphery of the reduced Brillouin zone we can obtain the bulk band structure. This, of course, leaves out Bloch vectors *inside* the irreducible zone. As an alternative description, all solutions within the Brillouin zone can be calculated and plotted as a function of k_y, with k_x as a parameter. We name the resulting band structure the *projected bands* along the k_y axis—the [010] direction of the Brillouin zone. Every projected band j occupies a band in the k_y-ω plane. The upper and lower edges of every band are characterized, respectively, by $k_x=0$ and $k_x=\pi/d$ or the reverse. By plotting the projected bands we can identify the frequency regions where the wave propagation is forbidden in the x,y plane. Upon crystal truncation with the cut plane parallel to the y,z plane, such regions of the k_y-ω plane are the forbidden gaps in which the surface modes can be found.

For the second case (the auxiliary structure), the complexity of the dielectric function of the supercell gives rise to a very complicated band structure. As for the bulk photonic bands, we also can calculate both the band structure along the periphery of the reduced zone of the Brillouin zone associated with the superstructure and the projected bands along the k_y axis. The latter, the projected band structure, represents an essential step of the supercell method. Performing calculations, we found groups of series of bands. Depending on the number of cylinders in the supercell, say, n, there appear groups each containing n bands. As n increases, each group becomes more and more compact and the band structure resembles the projected band structure of the infinite crystal (see the previous paragraph). Furthermore, when the conditions are appropriate, there appear additional bands lying in frequency regions where the wave propagation is forbidden in the x,y plane in the infinite crystal. Such bands are associated with surface modes of the crystal slab in the supercell. When the requirements for an accurate computation are satisfied (see Sec. I), these bands become very narrow and approach the dispersion curves of the surface modes of the semi-infinite crystal.

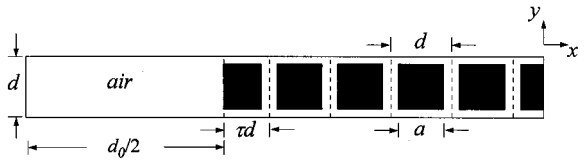

FIG. 2. One-half of the supercell. In this example the complete supercell [symmetric as shown in Fig. 1(b)] has $N=9$ complete cylinders and two incomplete cylinders of cross section $s(\tau)=s\times a$ $[s=\tau d-(d-a)/2]$. The supercell contains a row of cylinders bounded by air on both sides.

A. Bulk modes

The dielectric function of the unit crystal cell [Fig. 1(a)] is given by

$$\frac{1}{\varepsilon(x,y)} = \frac{1}{\varepsilon_b}+\left(\frac{1}{\varepsilon_a}-\frac{1}{\varepsilon_b}\right)\theta\left(\frac{a}{2}-|x|\right)\theta\left(\frac{a}{2}-|y|\right), \tag{6}$$

where $\theta(\alpha)$ is the Heaviside function ($\theta=1$ for $\alpha\geqslant 0$ and $\theta=0$ for $\alpha<0$). The Fourier coefficients are obtained from Eq. (5) as

$$\mu_{\mathbf{G}} = \left\{\frac{1}{\varepsilon_b}+\left(\frac{1}{\varepsilon_a}-\frac{1}{\varepsilon_b}\right)f\right\}\delta_{\mathbf{G},0} + \left(\frac{1}{\varepsilon_a}-\frac{1}{\varepsilon_b}\right)f\frac{\sin[G_x(a/2)]}{G_x(a/2)}\frac{\sin[G_y(a/2)]}{G_y(a/2)}(1-\delta_{\mathbf{G},0}), \tag{7}$$

where the packing fraction f is

$$f = \frac{a^2}{A_c} = \left(\frac{a}{d}\right)^2 \tag{8}$$

and the reciprocal lattice vectors are

$$\mathbf{G} = \frac{2\pi}{d}(m_x\hat{i}+m_y\hat{j}). \tag{9}$$

In principle, m_x and m_y assume all the integer values. To obtain the bulk band structure, we must substitute Eq. (7) into Eqs. (3) and (4).

B. Supercell representation for surface modes

In Fig. 2 we present the supercell used for calculations. This is a rectangular symmetric cell containing $n=9$ inner

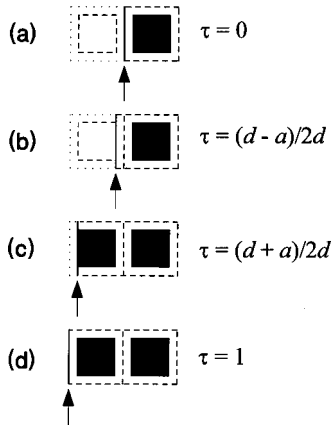

FIG. 3. Variation of the position of the surface plane, marked with a solid line and an arrow. The cell to the left (right) of this line is the surface cell (first bulk cell). (a) The crystal terminates with complete cells at the surface. (b) The host material forms a continuous layer of nominal (maximum) width at the surface. (c) The surface is tangent to the left face of the complete cylinder in the surface cell. (d) The crystal terminates again with complete cells at the surface; however, an additional cell has been added. Of course, for a crystal of dielectric rods in air all four terminations are equivalent. On the other hand, in a crystal of air cylinders only situations (a) and (d) are equivalent.

cylinders. The two last cylinders (one for each side of the crystal slab) can have equal or smaller cross section than the inner cylinders. This depends on the position of the cut plane. In order to study the properties of the surface modes as a function of the position of the surface, we used the cut parameter $\tau\,(0\leqslant\tau\leqslant 1)$.[3] The meaning of this parameter can be understood from Fig. 3. If $\tau=0$, the crystal terminates with complete cells [Fig. 3(a)]. As τ increases, the termination changes. For instance, with $\tau=0.5$ the surface cuts in half the last cells, leaving cylinders of half the nominal cross section. When $\tau=1$ the crystal slab has $n=9$ inner cylinders and two complete last cells [see Fig. 3(d)]. Of course, this case could be equally described by $n=11$ and $\tau=0$. If n is sufficiently large, then $\tau=0$ and $\tau=1$ give the same results.

For a given value of τ, the area of the last cell in the supercell is τd^2. For a supercell of length $L=(n+2\tau)d+d_0$ along the x axis and width $l=d$ along the y axis, we may write

$$\frac{1}{\varepsilon(x,y)}=\frac{1}{\varepsilon_0}+\left(\frac{1}{\tilde{\varepsilon}(x,y)}-\frac{1}{\varepsilon_0}\right)\theta\left(\frac{L-d_0}{2}-|x|\right), \tag{10}$$

where the dielectric function of the crystalline part (of length $L-d_0$) is

$$\frac{1}{\tilde{\varepsilon}(x,y)}=\frac{1}{\varepsilon_b}+\left(\frac{1}{\varepsilon_a}-\frac{1}{\varepsilon_b}\right)\times\left[\sum_{j=1}^{n}\theta\left(\frac{a}{2}-|x-x_j|\right)\theta\left(\frac{a}{2}-|y|\right)+F_\tau(x,y)\right]. \tag{11}$$

Here x_j represents the center positions of inner rods. The cut function F_τ is defined by

$$F_\tau(x,y)=\begin{cases}0, & 0\leqslant\tau<\dfrac{(d-a)}{2d},\\ \displaystyle\sum_{j=1}^{2}\theta\left(\frac{s}{2}-|x-x_j'|\right)\theta\left(\frac{a}{2}-|y|\right), & \dfrac{(d-a)}{2d}\leqslant\tau<\dfrac{(d+a)}{2d},\\ \displaystyle\sum_{j=1}^{2}\theta\left(\frac{a}{2}-|x-x_j'|\right)\theta\left(\frac{a}{2}-|y|\right), & \dfrac{(d+a)}{2d}\leqslant\tau<1.\end{cases} \tag{12}$$

In this equation $s=\tau d-(d-a)/2$ is the length along the x direction of the incomplete rods in the last layer and x_j' are the center positions of the two exterior rods—one for each surface layer delimiting the crystal slab. It is easy to show that $x_j'=\pm[(n+\tau)d/2+(d-a)/4]$ and $x_j'=\pm(n+1)d/2$ when the cut parameter corresponds to incomplete and complete rods at the surface, respectively.

The Fourier coefficients are found to be

$$\mu_{\mathbf{G}}=\left\{\frac{1}{\varepsilon_0}+\left(\frac{1}{\varepsilon_b}-\frac{1}{\varepsilon_0}\right)\frac{(L-d_0)d}{A_{sc}}+\left(\frac{1}{\varepsilon_a}-\frac{1}{\varepsilon_b}\right)\left[\frac{a^2}{A_{sc}}n+\mathcal{J}_1(\tau)\right]\right\}\delta_{\mathbf{G},0}+\left(\frac{1}{\varepsilon_b}-\frac{1}{\varepsilon_0}\right)\frac{(L-d_0)d}{A_{sc}}\frac{\sin[G_x(L-d_0)/2]}{G_x(L-d_0)/2}(1-\delta_{G_x,0})\delta_{G_y,0}$$

$$+\left(\frac{1}{\varepsilon_a}-\frac{1}{\varepsilon_b}\right)\left\{\frac{a^2}{A_{sc}}\frac{\sin(G_xa/2)}{G_xa/2}\frac{\sin(G_ya/2)}{G_ya/2}\sum_j\exp(iG_xx_j)+\mathcal{J}_2(\tau)\right\}(1-\delta_{\mathbf{G},0}), \tag{13}$$

where

$$\mathcal{J}_1=\begin{cases} 0, & 0\leqslant\tau<\dfrac{(d-a)}{2d}, \\ \dfrac{2sa}{A_{sc}}, & \dfrac{(d-a)}{2d}\leqslant\tau<\dfrac{(d+a)}{2d}, \\ \dfrac{2a^2}{A_{sc}}, & \dfrac{(d+a)}{2d}\leqslant\tau<1, \end{cases} \tag{14}$$

and

$$\mathcal{J}_2=\begin{cases} 0, & 0\leqslant\tau<\dfrac{(d-a)}{2d}, \\ \dfrac{sa}{A_{sc}}\dfrac{\sin(G_x s/2)}{G_x s/2}\dfrac{\sin(G_y a/2)}{G_y a/2}\displaystyle\sum_j \exp(iG_x x_j'), & \dfrac{(d-a)}{2d}\leqslant\tau<\dfrac{(d+a)}{2d}, \\ \dfrac{a^2}{A_{sc}}\dfrac{\sin(G_x a/2)}{G_x a/2}\dfrac{\sin(G_y a/2)}{G_y a/2}\displaystyle\sum_j \exp(iG_x x_j'), & \dfrac{(d+a)}{2d}\leqslant\tau<1. \end{cases} \tag{15}$$

In these equations, $A_{sc}=Ld$. Finally, the reciprocal lattice vectors are

$$\mathbf{G}=2\pi\left(\frac{m_x}{L}\hat{i}+\frac{m_y}{d}\hat{j}\right), \tag{16}$$

with m_x and m_y integer numbers.

III. NUMERICAL RESULTS

The frequency band structure shown in Fig. 4 corresponds to a crystal of square air cylinders in a background of dielectric constant $\varepsilon=17.9$ (GaSb at $\lambda=0.9\,\mu$m);[7] the packing fraction of the air is $f=0.67$. As can be seen, the crystal generates an absolute band gap for both TE (solid curves) and TM (dashed curves) polarizations. Therefore, the crystal is a good candidate to support surface modes of both polarizations. We have performed calculations for a truncated crystal with the surface plane parallel to the (100) plane. The propagation wave vector $\mathbf{k}_y$ lies along the [010] direction of the Brillouin zone.

In order to determine the available regions for the surface modes, in Fig. 5 we superpose the projected TE and TM frequency bands of both the crystal and air along the [010] direction. The line-shaded regions correspond to propagating solutions in the crystal—all electromagnetic modes within

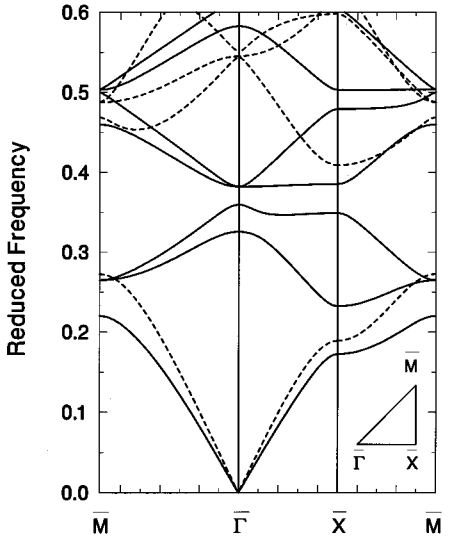

FIG. 4. Photonic band structure of a square lattice of square air cylinders. The dielectric constant in the interstitial region is $\varepsilon=17.9$, and the filling fraction (of the air) is $f=0.67$. The bands are plotted along the periphery of the irreducible Brillouin zone shown in the inset. The solid and dashed lines correspond to TE and TM polarizations, respectively. The crystal supports an absolute band gap (for propagation in the plane of periodicity) of width $\Delta\omega=0.022$ centered in $\omega=0.375$. The frequency is expressed in units of $(2\pi c/d)$.

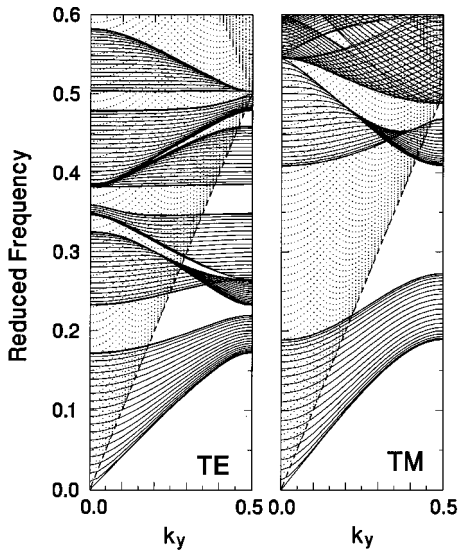

FIG. 5. Band projections along the y direction (the [010] direction of the 3D crystal). In each figure the line-shaded regions are the crystal bulk bands and the dot-shaded region is the air bulk band. The infinite air band is limited below by the light line $\omega=ck_y$. Only the gaps on the right side of the light line and above the lowest crystal band (four for TE modes and two for TM modes) are accessible for surface modes. The reduced wave vector k_y is in units of $(2\pi/d)$.

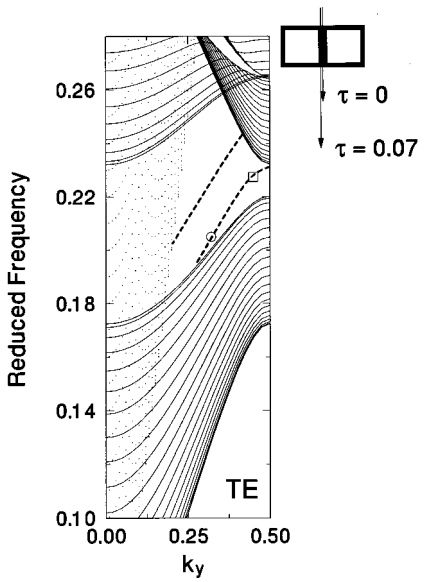

FIG. 6. Surface mode dispersion curves (dashed lines) in the first band gap for TE polarization. With complete cells at the surface ($\tau=0$), the surface modes lie roughly at the center of the gap. Given the small increment $\tau=0.07$, the modes are much lowered and emanate from the first bulk band, rather than from the light line. The figure demonstrates the strong sensitivity of the dispersion curve to the position of the surface.

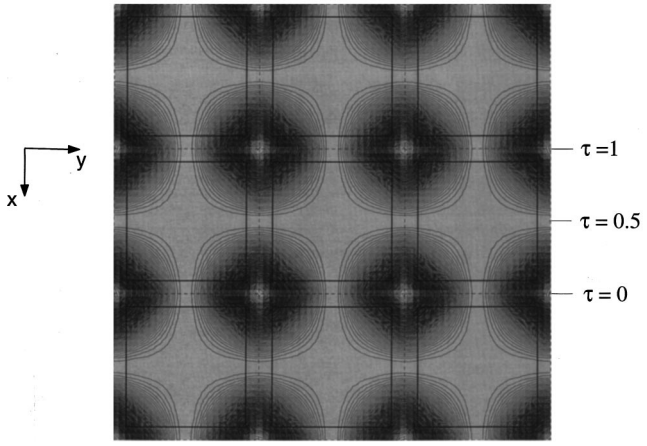

FIG. 7. Electric field intensity $|\mathbf{E}|^2$ contour map of the TE bulk mode for the lowest band at $k_x=k_y=\pi/d$ (the $\bar{M}$ point). Local minima (maxima) occur at the centers (corners) of the air cylinders—squares plotted with solid lines. The bulk band results from the coupling of all the local modes in the dielectric region. The truncation of the crystal with $\tau=0$ (or $\tau=1$) leaves strongly perturbed modes at the surface. These modes can not couple with the modes in the semi-infinite crystal and constitute a surface oscillation.

these bands have a real wave vector $\mathbf{k}=k_x\hat{i}+k_y\hat{j}$. The edges of the bands are defined by $k_x=0$ and $k_x=\pi/d$. On the other hand, the dot-shaded regions $\omega>ck_y$ satisfy the relation $\omega=c|\mathbf{k}+\mathbf{G}|$ corresponding to wave propagation in air (the interior of the light cone). This infinite band delimited below by the vacuum light line suffers a reflection at the limit of the Brillouin zone.

It is clear that solutions with fields decaying on both sides away from the surface can appear only in the crystal band gaps and outside the region for oscillating air solutions. In Fig. 5 we found four regions for TE modes and two regions for TM modes satisfying these conditions. In both cases the region below the lowest crystalline band is not available for physical solutions. We shall present results only for surface modes in the lowest band gaps.

Let us begin showing solutions for TE waves. In Fig. 6 we plot the dispersion curves of the surface modes for $\tau=0$ and $\tau=0.07$—the upper and lower dashed lines within the band gap, respectively. The position of the surface for each case is shown on the right side of the figure. With $\tau=0.07$ the incomplete surface cells have area$=0.07d^2$. The first thing to notice is the strong dependence of the dispersion curve on τ. The slight variation of the cut parameter moves the position of the curve to lower frequency values. We can observe that the modes near the light line disappear. The dispersion curve begins at $k_y\sim0.26$ at the top of the lower bulk band.

Previous works for crystals of dielectric rods supporting complete gaps have shown that the surface modes exist only for crystal terminations that leave incomplete cylinders at the surface.[4,5] Figure 6 shows that this is not true for crystals of air cylinders at least for the TE case. For crystals of dielectric rods, we can understand the origin of the surface modes as follows. It is known that the bulk band structure results from the overlapping of the electromagnetic modes of all the rods in the crystal. The coupling of the lowest mode of all the rods gives rise to the lowest band; the coupling of the second mode of all the rods gives rise to the second band, and so on. When the crystal is truncated with complete rods at the surface, the situation is not very different. Only the modes of the rods at the surface suffer a small perturbation because they are now in contact with the semi-infinite air-space interface. However, this perturbation is not sufficient to separate their modes from the band produced by the rest of the rods in the semi-infinite crystal. Only crystal truncation that leaves incomplete rods at the surface gives rise to new modes—essentially those of the rods of the last layer—which cannot couple to the bulk modes to form part of a band.

In our crystal of square air cylinders, the situation is different. Now the dielectric regions of neighboring cells are interconnected, producing stronger overlap of their modes. In particular, for the first bulk band we found that the fields have maximum amplitude at the corners of the unit cells (see Fig. 7). One might think that the band is produced by the interaction of the modes centered at the corners of all the cells. The termination of the crystal with $\tau=0$ leaves at the surface a continuous dielectric region of half the width of the internal dielectric regions, not unlike a waveguide. As occurs in the case of crystals with dielectric rods, the modes associated with this truncated region do not couple with the interior modes. These new modes of higher frequency remain detached as surface solutions lying above the ''valence band.''

The field confinement at the surface depends on the position of the mode in the forbidden gap. In Fig. 8 we present the field intensity at $y=0$ (the center of the supercell in the y direction) corresponding to the modes $k_y=0.32$, $\omega=0.21$ and $k_y=0.45$, $\omega=0.227$. We shall refer to these modes as the first and second modes, and we mark them with a circle and

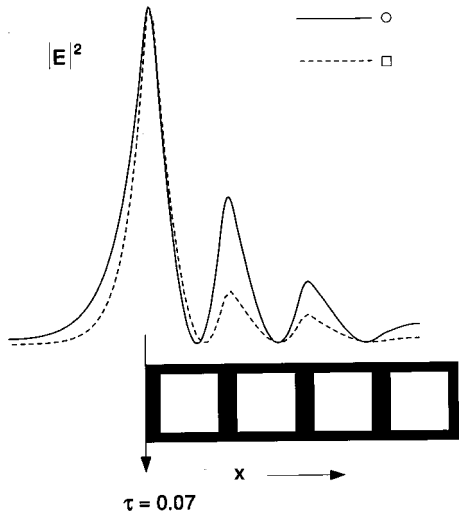

FIG. 8. Electric field intensity $|\mathbf{E}|^2$ at $y=0$ for the two surface modes marked in Fig. 6. The black squares below the curves are the air cylinders in the supercell. The arrow represents the position of the surface. On the air side the stronger confinement at the surface is obtained for the more distant point from the light line (the mode marked with a square in Fig. 6). On the crystal side the localization is stronger for the mode nearest the middle of the gap (again the mode marked with a square in Fig. 6).

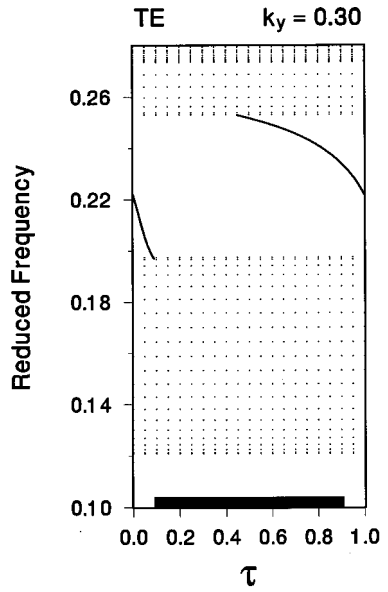

FIG. 9. TE surface modes behavior as a function of the cut parameter τ. The interval $0\leqslant\tau\leqslant1$ corresponds to the length of the unit cell in the x direction. The bar at the bottom of the figure represents the length of the air cylinder in the unit cell along the x axis. For the selected propagation vector $k_y=0.30$, the surface modes do not appear when the cut plane leaves the crystal with a narrow last row of cylinders, namely, for $0.09<\tau<0.42$.

a square, respectively, in the lower dispersion curve of Fig. 6. In this figure we observe that the first mode lies relatively near to the light line and near the edge of the first band. On the other hand, the second mode is far from both the light line and from bulk bands. What we learn from Fig. 8 is that the confinement at the surface of the second mode is better. As is the case for these two modes, we have found a general behavior: the fields of the surface modes are better localized at the surface when the modes lie far from the light line and close to the midgap.

The behavior on the air side can be understood considering that the decay distance is $\delta=2/[k_y^2-\omega^2/c^2]^{1/2}$ (k_y increases more than ω for the second mode, in comparison with the first mode). In order to understand the behavior of the fields inside the crystal, we remind the reader that the k_x component of any Bloch vector $\mathbf{k}=k_x\hat{i}+k_y\hat{j}$ within the band gap is complex. By increasing the frequency from the lower limit of the gap (for a fixed k_y), it is found that the imaginary part of k_x varies from 0 to a maximum value near the midgap. Then it decreases until 0 at the upper frequency limit of the gap. In this process the real part of k_x ($=\pi/d$) remains constant. The surface modes are electromagnetic oscillations guided by a real propagation vector k_y with the decay into the medium given by such a complex k_x. Because the decay distance is inversely proportional to the imaginary part of k_x, it is expected that modes nearer to the gap edges are more penetrating than the modes located at the midgap.

Another way to see the strong sensitivity of the surface modes to the termination of the crystal is shown in Fig. 9. In this figure we present the variation of the frequency of the surface mode as a function of the cut parameter τ for a fixed value of the propagation vector, namely, $k_y=0.30$. The bar on the τ axis [with ends at $\tau=(d-a)/2d=0.09$ and $\tau=(d+a)/2d=0.91$] represents the width of the air rods along the x axis (see Fig. 3). We can speak of three regions involved in the problem. In the first region where $0\leqslant\tau<0.09$, the surface mode exists for all τ. It lies in the lower half of the gap, disappearing just at the limit $\tau=0.09$. It is important to note that at this limit the dielectric layer at the surface has the full width that separates the air cylinders in the bulk. In the second region defined by $0.09\leqslant\tau\leqslant0.91$, a surface mode exist only for $\tau\geqslant0.45$. The frequency of the mode is lowered as τ increases. Finally, in the third region where $0.91<\tau\leqslant1$, the mode continues decreasing in frequency until reaching the value $\omega\cong0.22$, which, of course, coincides with the value for $\tau=0$. This is to say—at least for $k_y=0.3$—that a surface mode can be excited for every value of ω within the gap, provided that a suitable termination is chosen. Also, not surprisingly, if the surface cuts entirely through dielectric material, a surface mode can propagate. On the other hand, if the surface truncates the air cylinders, then there are no surface modes for relatively narrow cylinders ($\tau<0.45$).

Physically, by sweeping the cut parameter τ from 0 to 1 we add one mode—for each wave vector k_y in the Brillouin zone—to the lower band. The surface mode descends from the top of the band gap until it reaches the edge of the lower band, acquiring bulk mode properties. Although we have presented solutions only for the modes in the lowest band gap, similar behavior occurs within the higher-lying ones.

We now turn to discuss results for TM waves. In Fig. 10 we plot two dispersion curves for $\tau=0.5$ and $\tau=0.91$. The positions of the curves clearly show a strong dependence on τ. Searching for another branch for $\tau=0$, we have not found any solution. This observation provides the first, qualitative, difference between TE and TM modes in this crystal.

With respect to the confinement at the surface of the TM modes, we found the same behavior on the air side (as is expected) discussed above for TE waves. However, in the crystal the TM modes are less penetrating than the TE

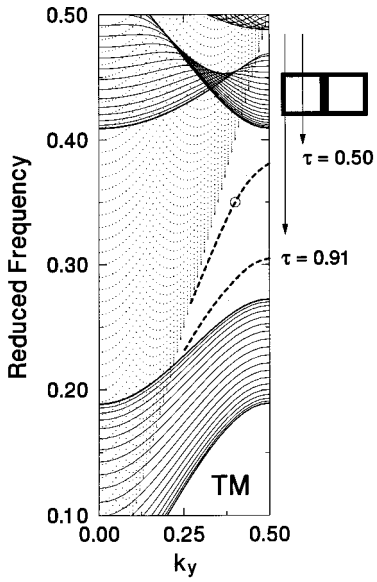

FIG. 10. Surface-mode dispersion curves (dashed lines) in the first band gap for TM polarization. Contrary to the TE case, TM surface modes do not occur when the crystal terminates with complete cells at the surface. The upper (lower) dispersion curve corresponds to a cut parameter $\tau=0.50$ (0.91).

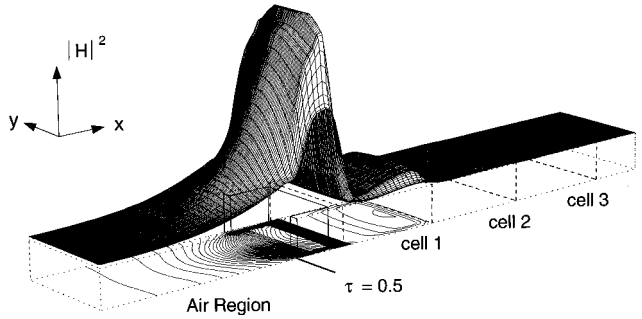

FIG. 11. Magnetic field intensity of the TM surface mode encircled in Fig. 10. The solid line outside the auxiliary ''basis'' indicates the position of the crystal-air interface. The dashed lines in the basis separate the unit cells of the crystal. The value $\tau=0.5$ means that the last cell is half truncated. The contour map of the field intensity is plotted at the bottom of the basis. It is interesting that the discontinuity at the top of the surface occurs at the end of the air region (which penetrates into the surface cell) rather than at the nominal surface.

modes. This is a second distinction between the TE and TM modes. In Fig. 11 we plot the field intensity $|\mathbf{H}|^2$ of the mode encircled in Fig. 10 ($k_y=0.40$, $\omega=0.35$). We observe that the field penetrates only as far as the second cell. We have not found such strong localization for any TE mode. Because the localization at the surface of the fields of any mode is related to the imaginary part of the Bloch wave vector, we conclude that in general this imaginary part is larger in the first TM gap than it is in the first TE gap.

Finally, a third difference can be found in the field profiles of TM and TE surface modes in the crystal. We have shown that the TE field has local maxima at the corners of the unit cells. For TM fields we find that the local maxima of the $|\mathbf{H}|^2$ field are located in the dielectric regions between neighboring rods (see Fig. 11).

IV. SUMMARY AND CONCLUSIONS

We have used the supercell method to derive both the dispersion curves and the field intensities of the surface electromagnetic waves that can propagate at the surface of a 2D photonic crystal. Calculations where performed for crystals of square cylinders arranged in a square lattice. The surface modes were obtained as a function of the position of the surface, namely, the position of the plane (with respect to a complete unit cell) that truncates the infinite crystal. For a crystal of air cylinders in a background of GaSb (whose band structure supports an absolute band gap), both TM and TE surface modes appear and their dispersion curves are strongly dependent on the position of the cut plane. Surface modes for the two polarizations exist (in the first band gaps of the respective band structure) for positions of the cut plane that leave the surface cylinders with cross sections larger than one-half of the nominal. However, when the surface takes the midposition between two cylinder layers (cutting entirely through the dielectric material), only the TE modes remain. By plotting the field intensities of modes located at different positions within the same gap, in general we found that the TM modes are more confined to the surface than the TE modes. Stronger field localization at the surface is obtained for modes lying far from the light line at the center of the band gap.

In a typical experimental situation, a plane wave is incident at the surface of the photonic crystal from the air side. If the angle of incidence is α, then the wave-vector component parallel to the surface is $q_y=(\omega/c)\sin\alpha$. A prism may be added in case of an attenuated total reflection (ATR) experiment, in which case this expression must be multiplied by the prism index. Because the crystal is periodic in the y direction, diffraction will generate partial modes with propagation vectors $k_y=q_y+(2\pi/d)n$, where n takes all the integer values. If $\omega<\pi c/d$, then k_y will fall outside the light cone for all values of n (provided that it is outside this cone for one value of n). Then the k_x (perpendicular) components in the air are pure imaginary for all n and the surface wave is a proper, nonradiative wave. On the other hand, if ω is greater than $\pi c/d$ (the frequency at which the light line crosses the edge of the first Brillouin zone), then k_y will fall inside the light cone for at least one value of n. As the frequency increases, this will occur for more and more n values, corresponding to increasing orders of diffraction. These partial waves will have real values of their k_x components and will contribute to radiation into the air. As a consequence, the surface wave will be damped. Such waves are called radiative or leaky. Because the dielectric contrast is usually very large in photonic crystals, the diffractive effects can be expected to be very strong, essentially destroying the surface wave. In this paper we investigated only nonradiative waves and also did not study the excitation due to an incident plane wave.

ACKNOWLEDGMENTS

This work was supported by Consejo Nacional de Ciencia y Tecnología, México, Grant No. 489100-5-3878PE. We also thank the Departamento de Cómputo Académico UNAM for its facilities.

[1] See papers in J. Opt. Soc. Am. B **10**, 283–413 (1993); *Photonic Band Gap Materials*, edited by C. M. Soukoulis (Kluwer Academic, Dordrecht, 1996); J. D. Joannopoulos, R. D. Meade, and J. N. Winn, *Photonic Crystals: Molding the Flow of Light* (Princeton University Press, Princeton, NJ, 1995); J. D. Joannopoulos, P. R. Villeneuve, and S. Fan, Nature (London) **386**, 143 (1997).

[2] K. M. Ho, C. T. Chan, and C. M. Soukoulis, Phys. Rev. Lett. **65**, 3152 (1990); E. Yablonovitch, T. J. Gmitter, and K. M. Leung, *ibid.* **67**, 2295 (1991); P. R. Villeneuve and M. Piché, Phys. Rev. B **46**, 4973 (1992); M. Plihal and A. A. Maradudin, *ibid.* **44**, 8565 (1991); V. Kuzmiak, A. A. Maradudin, and A. R. McGurn, *ibid.* **55**, 4298 (1997).

[3] R. D. Meade, K. D. Brommer, A. M. Rappe, and J. D. Joannopoulos, Phys. Rev. B **44**, 10 961 (1991).

[4] W. M. Robertson, G. Arjavalingam, R. D. Meade, K. D. Brommer, A. M. Rappe, and J. D. Joannopoulos, Opt. Lett. **18**, 528 (1993).

[5] F. Ramos-Mendieta and P. Halevi, Solid State Commun. **100**, 314 (1996).

[6] F. Ramos-Mendieta and P. Halevi, J. Opt. Soc. Am. B **14**, 370 (1997); Opt. Commun. **129**, 1 (1996).

[7] E. D. Palik, *Handbook of Optical Constants of Solids II* (Academic, Boston, 1991).